

Waves as the source of apparent twisting motions in sunspot penumbrae

L. Bharti¹, R.H. Cameron¹, M. Rempel², J. Hirzberger¹ and S. K. Solanki^{1,3}

1. Max-Planck-Institut für Sonnensystemforschung, Max-Planck-Str. 2, 37191

Katlenburg-Lindau, Germany

2. High Altitude Observatory, NCAR, P.O. Box 3000, Boulder, CO 80307, USA

3. School of Space Research, Kyung Hee University, Yongin, Gyeonggi Do, 446-701, Korea

bharti@mps.mpg.de

Received _____; accepted _____

Received; Accepted

ABSTRACT

The motion of dark striations across bright filaments in a sunspot penumbra has become an important new diagnostic of convective gas flows in penumbral filaments. The nature of these striations has, however, remained unclear. Here we present an analysis of small scale motions in penumbral filaments in both simulations and observations. The simulations, when viewed from above, show fine structure with dark lanes running outwards from the dark core of the penumbral filaments. The dark lanes either occur preferentially on one side or alternate between both sides of the filament. We identify this fine structure with transverse (kink) oscillations of the filament, corresponding to a sideways swaying of the filament. These oscillations have periods in the range of 5-7 min and propagate outward and downward along the filament. Similar features are found in observed G-band intensity time series of penumbral filaments in a sunspot located near disk center obtained by the Broadband Filter Imager (BFI) on board *Hinode*. We also find that some filaments show dark striations moving to both sides of the filaments. Based on the agreement between simulations and observations we conclude that the motions of these striations are caused by transverse oscillations of the underlying bright filaments.

Subject headings: Sun: sunspots

1. Introduction

High resolution Hinode and Swedish Solar Telescope observations of sunspots located away from disk center have revealed fine structure in penumbral filaments: filaments which are nearly perpendicular to the solar disk radius vector display a "twisting motion" indicated by dark striations moving across the filaments (i.e. perpendicular to the filament's axis) always directed from the limb-side to the center-side of the filament (Ichimoto et al. 2007). These striations can be used as tracers of the flow, and have observationally established the presence of overturning convection in the filaments (Zakharov et al. 2008; Bharti et al. 2010b), an idea which is consistent with theory and recent simulations (Heinemann et al. 2007; Rempel et al. 2009a,b). The direct measurement of the velocity is more difficult: Sánchez Almeida et al. (2007) found a local correlation between upflows and bright structures as well as between downflows and dark structures in a penumbra. Such correlations are suggestive of convective energy transport in the penumbra. The clear signal of an upflow along the central axis of a bright filament has been reported by Franz & Schlichenmaier (2009), Bellot Rubio et al. (2010) and Ichimoto (2010), downflows at its sides are more challenging to observe. Line syntheses from sunspot simulations (cf. Bharti et al. (2011)) suggest that these downflows are partly hidden in observations due to both limited spatial resolution, and the fact that commonly used lines form above the heights where the downflows are strongest. Moreover, the Evershed flow affects line of sight velocities, thus the detection of downflows at edges of filaments also depends on the location of the sunspot on the solar disk. Recently Joshi et al. (2011) and Scharmer et al. (2011) found downflows in dark regions at the edges of the penumbral filaments in the C I 5380 Å line formed deep in the photosphere. The results of these publications support the prediction made by Bharti et al. (2011). Scharmer & Henriques (2011) reported that downflows at the edges of filaments detected in the C I 5380 Å line (Scharmer et al. (2011)) are also present in the wing of Fe I 6301.5 Å with reduced amplitude.

The striations have the advantage that they potentially allow horizontal motions to be followed, if detected close to disk center, which would make them of unique diagnostic value for the velocity field we have. In previous studies by Ichimoto et al. (2007), Zakharov et al. (2008), Spruit et al. (2010) and Bharti et al. (2010b), the apparent twist of the striations was analyzed only in sunspots away from the disk center where the twisting motions is seen in filaments perpendicular to the line of symmetry (i.e. in filaments directed parallel to the nearest portion of the limb). The twists are always directed toward the center-side. This was interpreted as a geometrical effect by Zakharov et al. (2008) – these ”twisting” motions were exclusively interpreted in terms of overturning convective flows perpendicular to the filament’s major axis (Ichimoto et al. 2007; Zakharov et al. 2008; Scharmer 2009; Spruit et al. 2010). Spruit et al. (2010) proposed that these striations originate from the ”corrugation of the boundary between an overturning convective flow inside the filament and the magnetic field wrapping around it”. Based on their modeling results, they also argue that the striations are not compatible with a horizontal field along the axis of filaments in excess of 300 G. However, it is not certain if they really trace convective flows or not. This is an important point to establish, since the motions of the striations have been employed by Zakharov et al. (2008) to conclude that convective motions transport sufficient energy to explain the brightness of the penumbra (cf. Bharti et al. (2010b)) . In this paper we use the ”realistic” numerical radiative MHD simulations of (Rempel et al. 2009a,b; Rempel 2011) to investigate the causes of the observed brightness striations. In addition, we analyze such striations in penumbral structures observed at disk center and compare their properties with those found in the numerical simulations.

The paper is organized as follows: in Section 2 we describe the numerical simulation and present an analysis of the fine structure we find there, in Section 3 we describe the observations and compare the simulations with the observations. We then present our conclusions in Section 4.

2. Numerical simulations

The simulations analyzed here were carried out with the MURaM code (Vögler et al. 2005). The code includes the effects of partial ionization on the equation of state, and non-grey radiative transfer. For details of the code and the equations see Vögler et al. (2005) and for recent modifications, essential for the sunspot simulations presented here, see Rempel et al. (2009b). This code has been used extensively to treat problems both in the quiet Sun (Keller et al. 2004; Khomenko et al. 2005; Vögler & Schüssler 2007; Pietarila Graham et al. 2009, 2010; Danilovic et al. 2010a,b) as well as flux concentrations reaching from pores to entire active regions (Cameron et al. 2007; Cheung et al. 2008, 2010; Yelles Chaouche et al. 2009; Schüssler & Vögler 2006; Rempel et al. 2009a,b; Bharti et al. 2010a; Rempel 2010, 2011).

Here we present results from two different simulation runs. The first simulation uses a setup in 'slab' geometry, in which only a narrow slice through the center of a sunspot is simulated. The geometry and size of this simulation make it ideal for studying the detailed 3 dimensional evolution of individual penumbral filaments, albeit in a somewhat artificial geometry. The second simulation uses a setup with a pair of opposite polarity sunspots, leading to more extended penumbrae with a more realistic geometry.

2.1. Slab Geometry

A snapshot from the sunspot simulation in slab geometry described by Rempel et al. (2009b) was used as the initial condition for the calculations presented here. The simulation domain is periodic in both horizontal (x and y) directions, with dimensions of 4.6 Mm \times 36.864 Mm, and has a dimension of 6.144 Mm in the vertical (z) direction. The average value of the $\tau_{\text{Ross}} = 1$ ($\tau_{\text{Ross}} = 1$ levels refer to optical depth computed from the grey

opacities (which is Rossland mean opacity, an "average" opacity such that if we assume that the opacity at all frequencies is this average.)) height in the quiet Sun is used to define $z = 0$, and z is defined to be positive above this height and negative in the interior of the Sun. The vertical boundary conditions are unchanged from Rempel et al. (2009b): the top boundary is closed and the magnetic field above it is assumed to be potential. The bottom boundary is open as described in Vögler et al. (2005).

From this initial condition, the simulation was continued for 133 minutes of solar time, with snapshots saved every 34.5s.

2.1.1. *Simulation analysis*

The bolometric intensity of the entire simulation domain viewed from above at $t = 71.9$ min is shown in Fig. 1. Several penumbral filaments with central dark cores can be seen. In the following we consider the filament in the lower right region of the penumbra ($21.1 \leq y \leq 28.1$ Mm and $0 \leq x \leq 1.44$ Mm). A blow up of this region is shown in Fig. 2. There we see that, at the height of the cut $z = -384$ km (i.e. 384 km below the average $\tau_{\text{Ross}} = 1$ height of the quiet Sun) there is a continuous upflow along the central part of the filament and downflows along the borders. This cut lies below the local $\tau_{\text{Ross}} = 1$ surface, so that the shown up and downflows are not directly observable. The filament exhibits fine structure in the form of 'wiggles' in the bolometric intensity as well as horizontal and vertical velocities along its entire length. The wavelength in the x direction of the 'wiggles', at this fixed time, is approximately 700 km. Figure 3 shows that, when viewed at an angle, inclined striations which propagate away from the umbra appear, somewhat similar to what is seen in the high resolution observations by Ichimoto et al. (2007), Zakharov et al. (2008), Spruit et al. (2010) and Bharti et al. (2010b).

In order to study the time evolution of the fine structure, we first focus on cuts across the filament at $x = 25.7$ Mm. The time evolution of the cuts for various quantities are shown in Fig. 4. The range of the intensity image has been restricted in order to better reveal the fine structure between $t = 50$ and $t = 90$ min. Between $t = 0$ and $t = 30$ min there are clear variations in the intensity producing an asymmetric fishbone pattern, as dark lanes propagate first to one edge of the filament, then to the other. Somewhat weaker oscillations occur between 50 and 80 minutes, and these are followed by larger amplitude oscillations from $t \approx 100$ min onwards.

These bolometric intensity variations correspond to variations in the vertical velocity, with the minima in intensity corresponding to stronger downflows. These fluctuations are accompanied by variations in the y component of the velocity, corresponding to the tube at this height swaying first in the negative y direction, and then in the positive y direction. The second, weaker burst of oscillations occurs between $t = 50$ and $t = 90$ min. The intensity fluctuations associated with this second set of oscillations are more pronounced for $y < 700$ km. The weak velocity fluctuations, again best seen in v_y , indicate a swaying of the tube in the y direction, consistent with magnetic field strength variations which are asymmetric. The period of the oscillations in both phases is about 8 min. We emphasize that the perturbations occur across the entire inhomogeneous filament, despite the tube having very different velocities at different locations.

The vertical structure of v_y , as a function of time at the three points indicated by stars in Fig. 2 is shown in Fig. 5. At $x = 25.7$ Mm, $y = 510$ km (top frame of Fig. 5), we see that mostly $v_y < 0$, corresponding to an outflow away from the central axis of the filament. At $x = 25.7$ Mm, $y = 660$ km (middle panel), we see that along the center of the filament neither flows in the positive or negative y direction dominate and the clearest signature is of oscillatory motions. The situation at $x = 24.5$ Mm, $y = 810$ km (bottom panel of Fig.

5) is conceptually similar to that at $y = 510$ km, except that on this side of the filament $v_y > 0$ mostly dominates which again corresponds to a lateral outflow from the filament. Oscillatory motions can be seen, and are in phase at $y = 510$ km and $y = 660$ km, and especially at early times at $y = 810$ km. The oscillations are mainly propagating downwards (towards lower z at later times). We measured the wavelength to be ≈ 730 km.

As well as studying the x dependence of the oscillations at a particular time as in Fig. 2, we also took a space-time cut along the violet line in Fig. 2. This cut is shown in Fig. 6. The red line is placed at 25.7 Mm, corresponding to the red line in Fig. 2. Oscillations can be seen near the red line between $t = 0$ and $t = 30$ min and between $t = 50$ and $t = 90$ min. They appear as light and dark ridges running from the umbral end of the filament towards the granulation. The apparent x component of the wavelength is on the order of 1Mm.

The phase speed of the oscillations $\omega/\sqrt{k_x^2 + k_z^2}$ is then approximately 2 km/s. The wavevector, $(k_x, 0, k_z)$, is inclined by approximately 45° to the vertical, directed downwards and away from the umbra. The latter is consistent with the fact that the striations, when observed near the limb, appear to propagate only away from the umbra.

To visualize the waves, Fig. 7 shows the temperature in vertical cuts through the filament at the location indicated by the red line in Fig 2 at $t = 11$ and $t = 16.5$ min, corresponding to two nearly opposite phases of the oscillations. The differences in the temperature structure at the two phases is large in the top 200 km of the filament, indicating that the oscillations are outside the linear regime.

We comment that the mode is global with respect to the penumbral filament, although the filament has strong velocity, temperature and field gradients. For this reason we think it is dangerous to interpret the associated intensity fluctuations, such as those plotted in the top left of Fig. 6, as simple tracers of the velocity field.

There are numerous physical forces and processes which affect the oscillations. The period of 8 minutes (similar to the lifetime of granules) is long enough to make radiative processes important, the magnetic field is strong and structured, the flows are a significant fraction of the local sound speed and highly structured, whilst the density varies strongly across the filament and with depth. We leave the difficult task of disentangling the various waves and instabilities which could play a role to a future study.

2.2. Round sunspots

To see if the oscillations found above are specific to penumbral filaments in the slab geometry, we looked for similar features in the sunspot simulation described in Rempel et al. (2009a); Rempel (2011). The simulation domain is periodic in both horizontal directions (x and y), with dimensions of $98.304 \text{ Mm} \times 49.152 \text{ Mm}$, and has a vertical (z) extent of 6.144 Mm . The boundary conditions are identical to the slab simulation described above. The setup of this simulation contains a pair of opposite polarity sunspots with about $1.6 \cdot 10^{22} \text{ Mx}$ each and maximum field strengths of about 3 and 4 kG, respectively. This setup leads to an extended penumbra in between both spots and we focus here our investigation on a part of the penumbra belonging to the (left side) for the 4 kG sunspot (see, e.g., Figs. 1 of Rempel et al. (2009a); Rempel (2011, see, e.g., Figs. 1 of)). This part of the penumbra is the most extended displaying long, well formed fibrils, which are shown in Fig. 8. A detailed analysis of this region was recently performed by Rempel (2011).

The spatial location of the space-time slices plotted in Fig. 9 is marked by the horizontal line in Fig. 8. The time slices displayed in Fig. 9 are computed using a constant geometrical height about 300 km beneath the quiet Sun $\tau = 1$ level, which is below the local $\tau = 1$ in bright filaments and above it in the dark filaments. The presence of oscillations in this simulation is suggested by the typical asymmetric fishbone pattern, earlier detected in

the slab simulation, most clearly visible in the filament at the position $x = 9$ Mm. This suspicion is heightened by the clear oscillatory signal in the velocity perpendicular to the filament. A more detailed view of the filaments located between $x = 2.25$ and $x = 5.25$ Mm as well as $x = 8.1$ and $x = 9.9$ Mm is shown in Figs. 10 and 11, respectively. Clearly, this simulation also displays oscillations in several filaments in the innermost parts of the penumbra with periods around 7-8 minutes. The most significant difference compared to the oscillations in the slab geometry is a substantially smaller horizontal displacement. While the slab simulation presented in Fig. 4 shows a lateral displacement of the filament with an amplitude comparable to the width of the filament in all plotted variables, the oscillations here occur within otherwise mostly unaffected flow channels. The oscillation is most prominent in the intensity and in the velocity component lateral to the filament. Variations in the magnetic field strength are mostly restricted to a narrow boundary layer characterized by enhanced horizontal and reduced vertical field strength. This boundary layer coincides with the region of convective downflows at the edge of the filaments, as has been shown in Rempel (2011, see Fig. 17 therein). The vertical flow velocity shows moderate changes in the central upflows, but a rather intermittent behavior in the lateral downflows. The average outflow velocity from filament has its largest amplitudes near the outer edge of the filaments, where we also find the strongest flow variations. They remain small compared to the mean flow velocity, however. Both, the radial magnetic field and radial outflow originate mostly from a thin boundary layer just below the $\tau = 1$ level (see Fig. 17 of Rempel 2011), where strong horizontal field is induced and the Evershed flow is driven. The horizontal field and accelerated fluid are transported downward by the overturning convection within the filament, leading in deeper layers to a filament structure with enhancements of both radial magnetic field strength and flow velocity at the lateral boundaries of the filaments. The most significant difference between this simulation and the previously discussed slab simulation is in terms of a substantially stronger Evershed flow

that is accompanied with stronger horizontal field within flow channels: the flow velocity along filaments reaches in most filaments 3 km/s, while the horizontal field strength remains of the order of 1.5 kG. The horizontal field enhances the stiffness in the direction along filaments and thus suppresses lateral deformations. This could be taken as an indication that the lateral displacement of the flow channel in Fig. 4 is more a consequence than a cause of the oscillation mode. Furthermore the substantial difference in flow velocity and field strength does not seem to affect the oscillation period compared to the example shown in Fig. 4.

3. Observations

For the present study we selected a time series of G-band (4305 Å) images of a sunspot located almost at disk center and recorded by the Broadband Filter Imager (BFI) of the Solar Optical Telescope (SOT) onboard *Hinode* (Tsuneta et al. 2008). Such a location differs significantly from all previous studies of moving dark stripes in penumbral filaments, which were all carried out closer to the limb. The time series, recorded on January 5, 2007, consists of 432 images at 30 s cadence and contains a sunspot (NOAA 10933) located at disk center. The spatial resolution in the G-band is approximately $0''.22$. The image scale is $0''.054$ per pixel. The Solar Soft pipelines for the *Hinode* SOT/BFI were used for flat field and dark current corrections. The images are reconstructed for the instrumental PSF, applying a Wiener filter (Sobotka et al. 1993) and assuming diffraction on an ideal circular 50 cm aperture. Finally, a subsonic filter (Title et al. 1989) with a cut-off velocity of 6 km s^{-1} is used to filter out contributions of five-minute oscillations. The first and last 14 images from the time series of January 5, 2007 have been omitted due to the apodizing window used in the subsonic filtering. The mean intensity of quiet regions (i.e., regions containing undisturbed granulation and an absence of bright points) close to the observed

sunspot were used for intensity normalization in all images.

3.1. Observational analysis

Figure 12 shows a G-band image of the sunspot at the beginning of the filtered time series. A central umbra and a fully developed penumbra can be seen. Filaments oriented in all azimuthal directions clearly exhibit central dark cores. An animation of the analyzed time series reveals a lateral motion of dark lanes in the filaments from the axis of a particular filament toward either one of its edges, or toward both of its edges. These lateral motions are found in all azimuthal directions from the center of the sunspot. They are strongest at the inner ends of the filaments, in particular in filaments that protrude into the umbra.

Two representative space-time diagrams are shown in Figs. 13 and 14, respectively. they correspond to the lines 'S1' and 'S2' lying on opposite sides of the penumbra in Fig. 12. The motion of thin dark stripes across some of the filaments is apparent as inclined dark stripes in Figs. 13 and 14.

Figure 13 shows the space time diagram for the horizontal slit 'S1'. The white boxes indicate locations of filaments where inclined stripes or "twists" can be clearly seen. Only some of the filaments show such stripes and only for a part of the time. In the panels on the right, each box is displayed two times, once simply to highlight the stripes, the second time with white lines overplotted on the dark stripes for better visibility. Filament 'A', located at $x = 19''.5$, shows a central dark core and dark stripes, from 0 to 20 min, pointing toward both edges. The dark stripes in opposite directions occur alternatively, recalling from the spacing between asymmetric fishbone appearance already seen in the left panel of Fig. 4. This pattern can also be seen for filament 'B' at $x = 23''.5$ from 22 to 38 min. Filament 'C' at $x = 27''.0$ shows stripes in one direction only. Filament 'D' located at $x = 23''.0$

shows dark stripes from 100 to 135 min also just in one direction, but opposite to 'C'. Such "one-sided" stripes may correspond to the weaker, asymmetric oscillations seen between 50 and 90 min in the slab simulations (Fig. 3) and the leftmost filament located between 2.5 to 3.0 Mm in Fig. 9 for the round spot.

Figure 14 is a space-time plot along slit 'S2' depicted in Fig. 12. Filament 'E', located at $x = 27''0$, shows stripes in one direction from 30 to 75 min. Filament 'F' at $x = 29''5$ shows an asymmetric fishbone pattern from 56 to 70 min. Figure 14 demonstrates that such stripes are not restricted to a single location and that, because the sunspot is nearly at disk center, opposite sides of the penumbra display essentially the same behavior (in a statistical sense). From these two images we estimate that the period of the observed oscillations is in the range of 3 to 7 minutes.

Space-time diagrams along further lines (slits) cutting across filaments slits oriented perpendicular to S1 and S2 (e.g. at solar $x = -22$ and at $+4$ arc sec) were also produced (not shown). Similar stripes and patterns as shown in Figs. 13 and 14 can also be recognized there, although slightly less clearly.

It is also instructive to consider space-time diagrams running along the filaments (i.e. along slit S3 in Fig. 12), the observational analogy to that shown for the simulation in Fig. 6. The oscillations we saw in Figs. 13 and 14 are also visible in Fig. 15. They can be clearly seen between $y = -35$ and $y = -34$ arsec between $t = 0$ and $t = 30$ as a stack of dark and white stripes, whose inclination to the horizontal indicates that the waves are propagating outwards from the umbra. However, it is also clear that oscillations and propagating waves are ubiquitous. In particular, on the opposite side of the umbra waves (now propagating in the opposite direction, i.e. still away from the umbra) are visible at many locations. From this figure we can also determine that the wavelength along the filament is about 500 km.

Not only are moving stripes visible also at disk center and not just at the limb, but they also move with roughly the same phase-speed ($1.2\text{-}2.8\text{ km s}^{-1}$) and display roughly the same periodicity (3-7 min) at disk center as they do closer to the limb. This observed velocity is consistent with the apparent phase velocity inferred from the simulation, e.g. 2 km s^{-1} for the slab geometry (see Section 2.1.1), although the period is somewhat larger in the simulations (possibly related to the subsonic filtering we applied to the observations), e.g. 8 min in the slab geometry and 7-8 min for the round sunspots.

4. Conclusion

We analyzed striations moving across bright penumbral filaments in both numerical simulations and in a time series of seeing-free G-band images obtained with *Hinode*. In both cases we find that these moving striations, which give the filaments a twisting appearance, are also visible at disk center and appear relatively similar in simulations and observations. Interestingly, at disc center the two halves of a filament on either side of its central dark core can display "twists" in opposite directions, with the stripes on the two sides being out of phase.

Two different numerical simulations indicate that the striations are oscillations propagating along the penumbral filaments directed away from the umbra and downward. The periods of the oscillations one found to be 3-7 min from observations and 7-8 min in the simulations. The explanation for the striations suggested by the simulations is quite different from that proposed by Spruit et al. (2010) and, in particular does not support their conclusion that the striations imply the absence of a dynamically significant horizontal magnetic field strength in bright penumbral filaments. The MHD simulations reproduce the data rather well, although they have a rather dynamically significant horizontal field in the filaments. Although the Simulations with a stronger horizontal field (1500 G) in

the filaments produce oscillations with a smaller amplitude, they are still consistent with the observations. These oscillations are potentially a new seismic diagnostic which can be used to better understand penumbral filaments. This would, however, require a physical understanding of the underlying oscillatory mode, which itself will require further study.

This work has been partly supported by the WCU grant No. R31-10016 funded by the Korean Ministry of Education, Science and Technology. Hinode is a Japanese mission developed and launched by ISAS/JAXA, collaborating with NAOJ as a domestic partner, NASA and STFC (UK) as international partners. Scientific operation of the Hinode mission is conducted by the Hinode science team organized at ISAS/JAXA. Support for the post-launch operation is provided by JAXA and NAOJ (Japan), STFC (U.K.), NASA (U.S.A.), ESA, and NSC (Norway). The National Center for Atmospheric Research is sponsored by the National Science Foundation. Computing time was provided by NCAR's Computational and Information Systems Laboratory (CISL).

REFERENCES

- Bellot Rubio, L. R., Schlichenmaier, R., & Langhans, K. 2010, *ApJ*, 725, 11
- Bharti, L., Beeck, B., & Schüssler, M. 2010a, *A&A*, 510, A12+
- Bharti, L., Schüssler, M., & Rempel, M. 2011, *ApJ*, 739, 35
- Bharti, L., Solanki, S. K., & Hirzberger, J. 2010b, *ApJ*, 722, L194
- Cameron, R., Schüssler, M., Vögler, A., & Zakharov, V. 2007, *A&A*, 474, 261
- Cheung, M. C. M., Rempel, M., Title, A. M., & Schüssler, M. 2010, *ApJ*, 720, 233
- Cheung, M. C. M., Schüssler, M., Tarbell, T. D., & Title, A. M. 2008, *ApJ*, 687, 1373
- Danilovic, S., Schüssler, M., & Solanki, S. K. 2010a, *A&A*, 509, A76+
- . 2010b, *A&A*, 513, A1+
- Franz, M. & Schlichenmaier, R. 2009, *A&A*, 508, 1453
- Heinemann, T., Nordlund, Å., Scharmer, G. B., & Spruit, H. C. 2007, *ApJ*, 669, 1390
- Ichimoto, K. 2010, in *Magnetic Coupling between the Interior and Atmosphere of the Sun*, ed. S. S. Hasan & R. J. Rutten, 186–192
- Ichimoto, K., Suematsu, Y., Tsuneta, S., Katsukawa, Y., Shimizu, T., Shine, R. A., Tarbell, T. D., Title, A. M., Lites, B. W., Kubo, M., & Nagata, S. 2007, *Science*, 318, 1597
- Joshi, J., Pietarila, A., Hirzberger, J., Solanki, S. K., Aznar Cuadrado, R., & Merenda, L. 2011, *ApJ*, 734, L18+
- Keller, C. U., Schüssler, M., Vögler, A., & Zakharov, V. 2004, *ApJ*, 607, L59
- Khomenko, E. V., Shelyag, S., Solanki, S. K., & Vögler, A. 2005, *A&A*, 442, 1059

- Pietarila Graham, J., Cameron, R., & Schüssler, M. 2010, *ApJ*, 714, 1606
- Pietarila Graham, J., Danilovic, S., & Schüssler, M. 2009, *ApJ*, 693, 1728
- Rempel, M. 2010, ArXiv e-prints
- . 2011, *ApJ*, 729, 5
- Rempel, M., Schüssler, M., Cameron, R. H., & Knölker, M. 2009a, *Science*, 325, 171
- Rempel, M., Schüssler, M., & Knölker, M. 2009b, *ApJ*, 691, 640
- Sánchez Almeida, J., Márquez, I., Bonet, J. A., & Domínguez Cerdeña, I. 2007, *ApJ*, 658, 1357
- Scharmer, G. B. 2009, *Space Sci. Rev.*, 144, 229
- Scharmer, G. B. & Henriques, V. M. J. 2011, ArXiv e-prints
- Scharmer, G. B., Henriques, V. M. J., Kiselman, D., & Rodríguez, J. d. l. C. 2011, *Science*, 333, 316
- Schüssler, M. & Vögler, A. 2006, *ApJ*, 641, L73
- Sobotka, M., Bonet, J. A., & Vazquez, M. 1993, *ApJ*, 415, 832
- Spruit, H. C., Scharmer, G. B., & Löfdahl, M. G. 2010, *A&A*, 521, A72+
- Title, A. M., Tarbell, T. D., Topka, K. P., Ferguson, S. H., Shine, R. A., & SOUP Team. 1989, *ApJ*, 336, 475
- Tsuneta, S., Ichimoto, K., Katsukawa, Y., Nagata, S., Otsubo, M., Shimizu, T., Suematsu, Y., Nakagiri, M., Noguchi, M., Tarbell, T., Title, A., Shine, R., Rosenberg, W., Hoffmann, C., Jurcevich, B., Kushner, G., Levay, M., Lites, B., Elmore, D.,

Matsushita, T., Kawaguchi, N., Saito, H., Mikami, I., Hill, L. D., & Owens, J. K. 2008, *Sol. Phys.*, 249, 167

Vögler, A. & Schüssler, M. 2007, *A&A*, 465, L43

Vögler, A., Shelyag, S., Schüssler, M., Cattaneo, F., Emonet, T., & Linde, T. 2005, *A&A*, 429, 335

Yelles Chaouche, L., Cheung, M. C. M., Solanki, S. K., Schüssler, M., & Lagg, A. 2009, *A&A*, 507, L53

Zakharov, V., Hirzberger, J., Riethmüller, T. L., Solanki, S. K., & Kobel, P. 2008, *A&A*, 488, L17

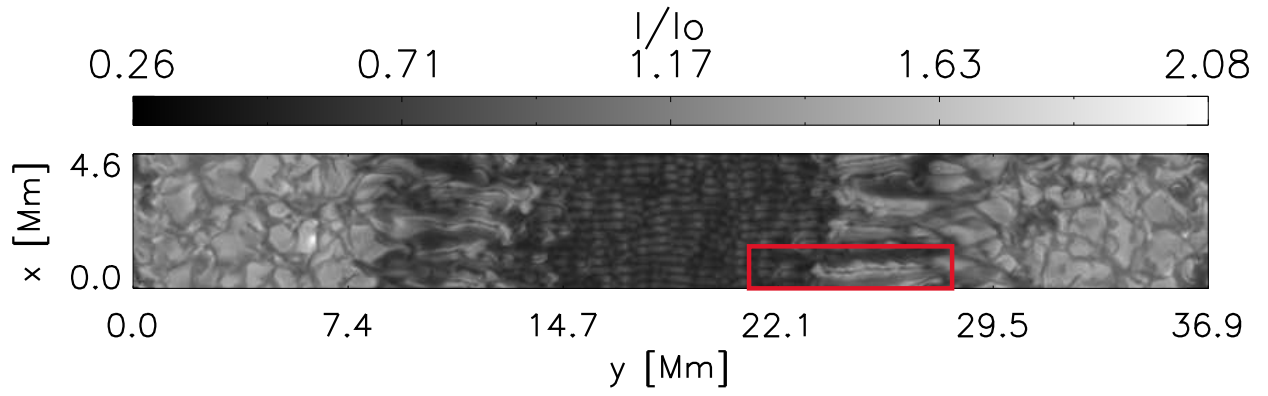


Fig. 1.— Bolometric intensity from the simulation in slab geometry at $t = 71.9$ min. The red box indicates the filament we chose for further study.

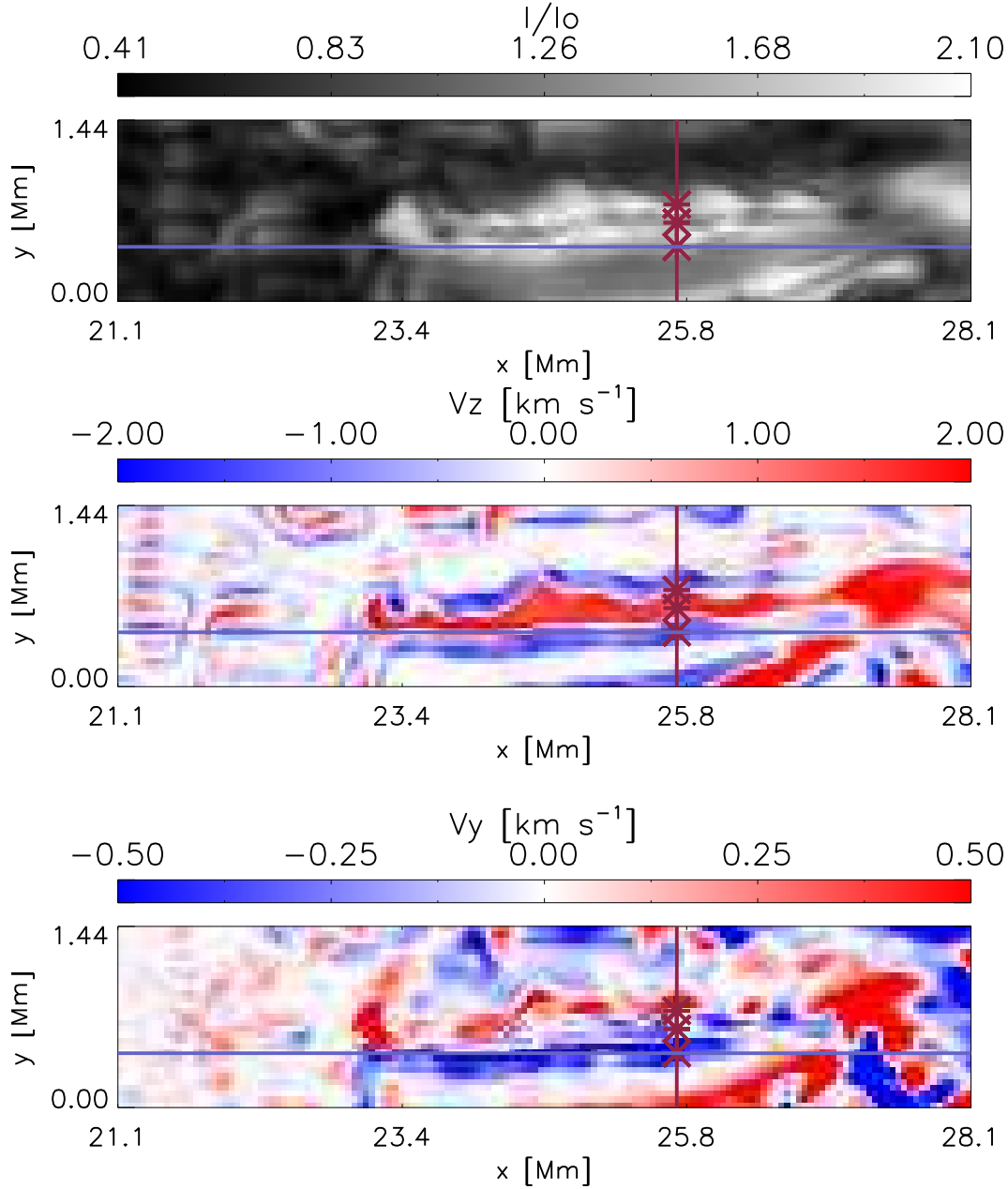


Fig. 2.— Intensity map and horizontal cuts through the simulated filament in the red box in Fig 1. From top to bottom, the panels show: the bolometric intensity; the component of the velocity in the y direction saturated at -500 m/s (red) and $+500$ m/s (blue) at a height $z = -384$ km below the average height of $\tau_{\text{Ross}} = 1$ in the quiet Sun ; and the component of the velocity in the z direction saturated at -2 km/s (red) and $+2$ km/s (blue) at the same height. The red line at $x = 25.6$ Mm, the red crosses and the blue line at $y = 0.51$ Mm show the locations at which slices were taken for further analysis (black in lower frames).

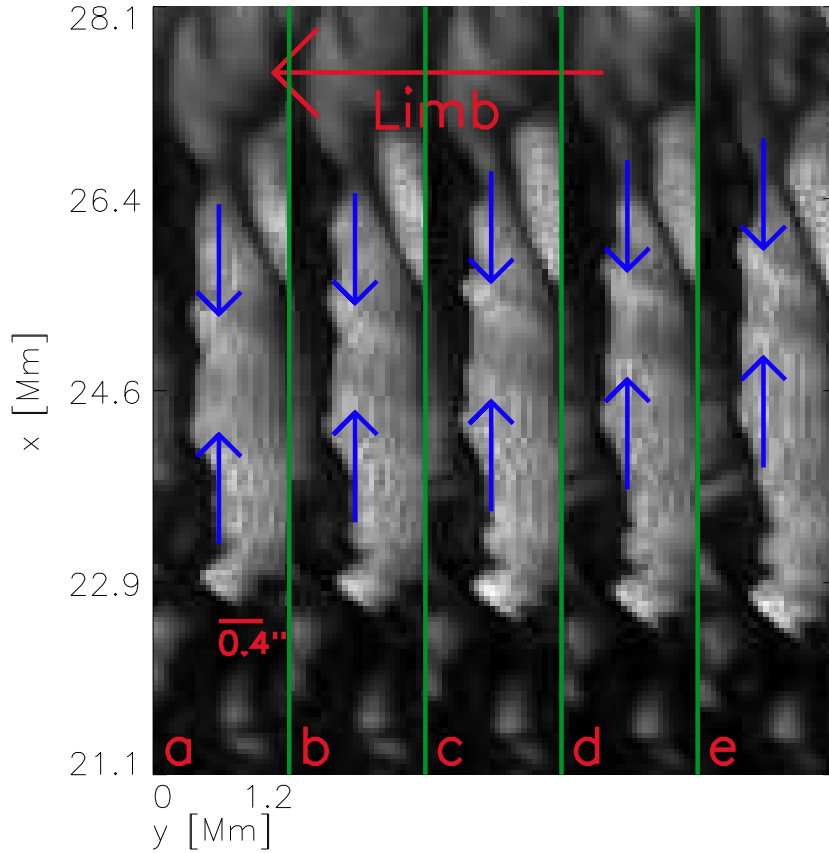


Fig. 3.— Snapshots of the simulated penumbral filament seen at an angle of 50° from disk centre at times (a) $t = 57$ min, (b) 60 min, (c) 63 min, (d) 66 min and (e) 69 min. The umbra is situated at the bottom of the figure and the quiet-Sun above the top of the figure. At this viewing angle, inclined striations, indicated by the blue arrows, can be seen propagating away from the umbra.

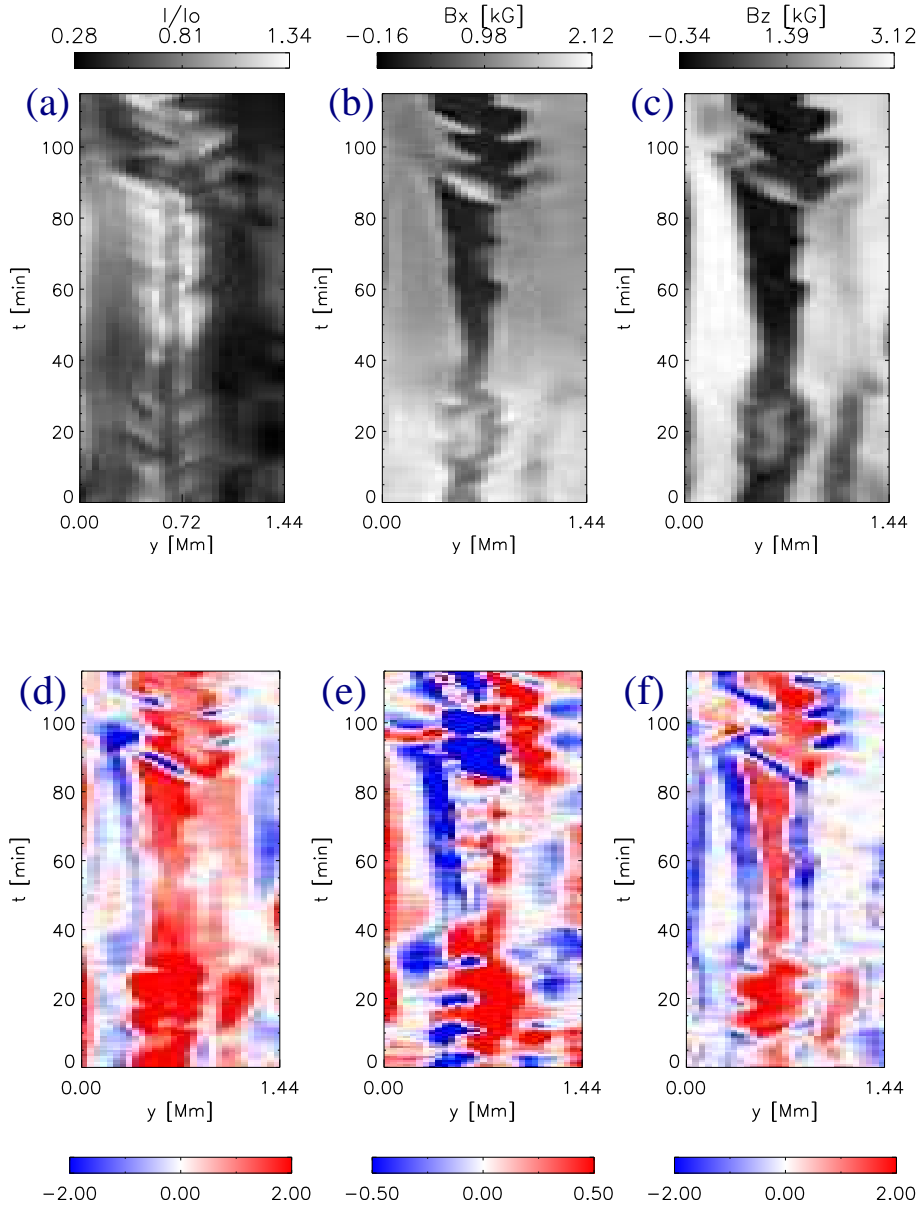


Fig. 4.— Space-time plots from the MHD simulations at the slit location marked in red in Fig. 2(top panel). Shown are (a) the bolometric intensity, (b) the x component of the magnetic field, (c) the vertical component of the magnetic field, (d) the x component of the velocity, (e) the y component of the velocity, and (f) the vertical component of the velocity. The last five quantities are sampled at a constant geometric height of $z = -384$ km below the average τ_{Ross} height of the quiet Sun.

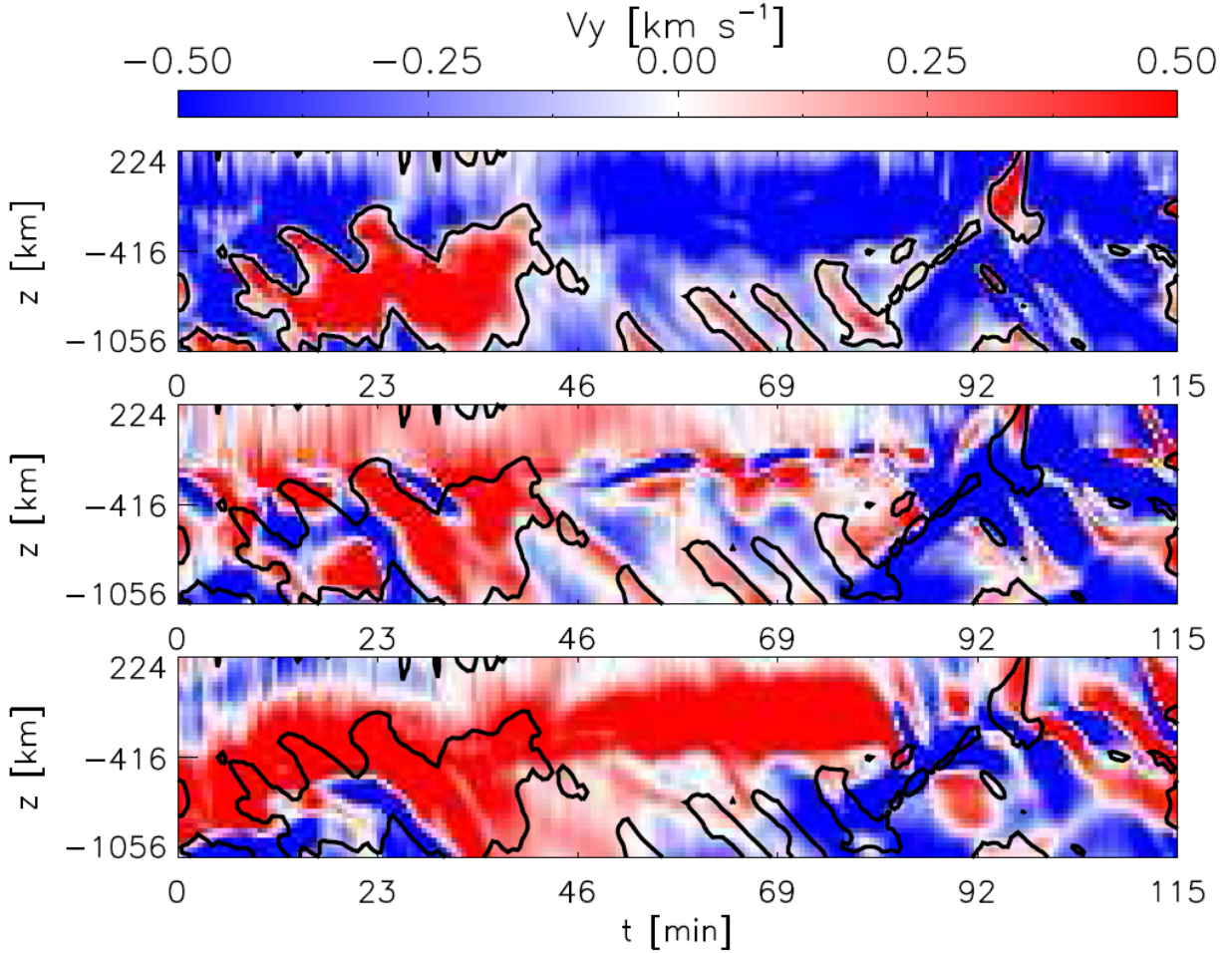


Fig. 5.— Space-time plots from the MHD simulations at the three locations marked by crosses along the slit marked in Fig. 2, i.e. from top to bottom at $y = 510$ km, $y = 660$ km and $y = 810$ km, respectively. The spatial dimension corresponds to height, with $z = 0$ corresponding to the average value of $\tau_{\text{Ross}} = 1$ in the quiet Sun. Positive values of z correspond to heights above the quiet-Sun $\tau = 1$ level. The y component of the velocity, saturated between ± 500 m/s, is shown. The black lines show where $v_y = 0$ at $y = 510$ km, they are intended to provide a reference for comparing the structure of the velocity field between all three sub-images.

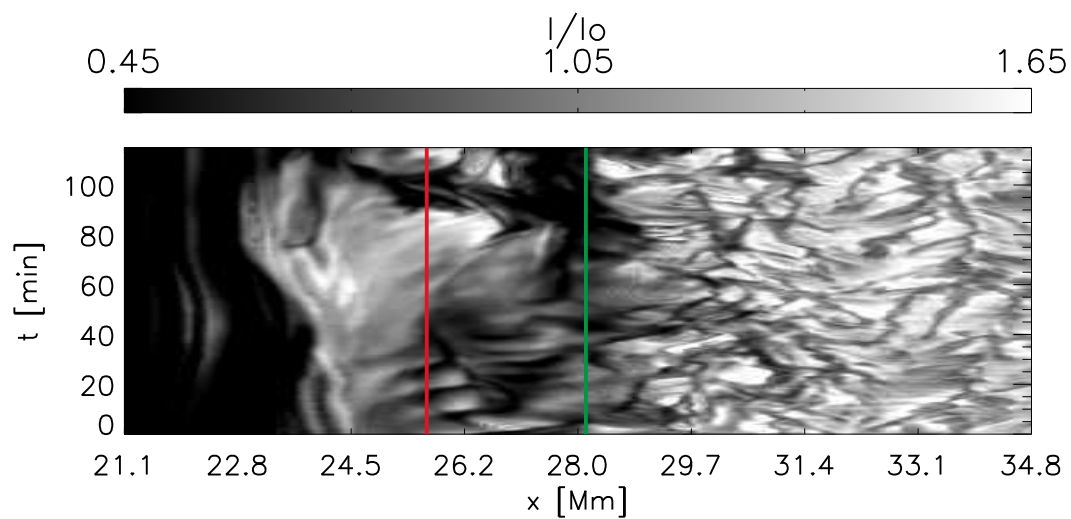


Fig. 6.— Space-time plots of the normalized bolometric intensity along the blue line shown in Fig. 2 extended into the ‘quiet-Sun’ granulation. This cut is along the penumbral filament, but offset from the centre of the filament. The red line shows the x value used to make Figures 4, and 5. To give an impression of how the signal discussed here differs from that of the umbra and quiet Sun, we have used a bigger box than that used in Fig. 2, with the green line showing the extent of the box shown in Fig. 2.

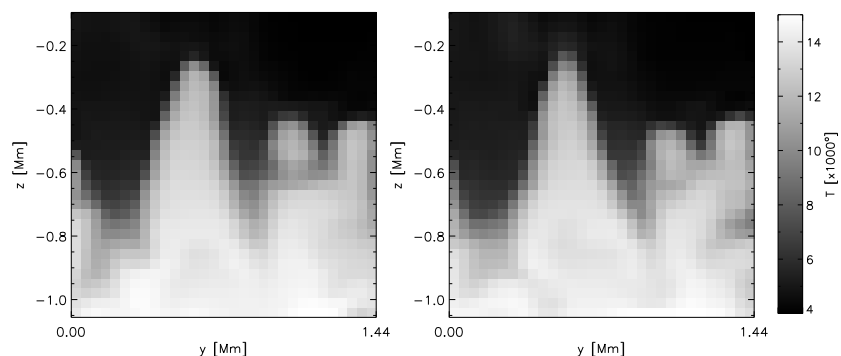


Fig. 7.— Vertical cuts through the temperature field of the filament shown in Fig. 2 at different phases of the oscillation, $t = 11$ min (left panel) and $t = 16.7$ (right). The average height of $\tau_{Ross} = 1$ in the quiet Sun was used to define $z = 0$, with z increasing outwards.

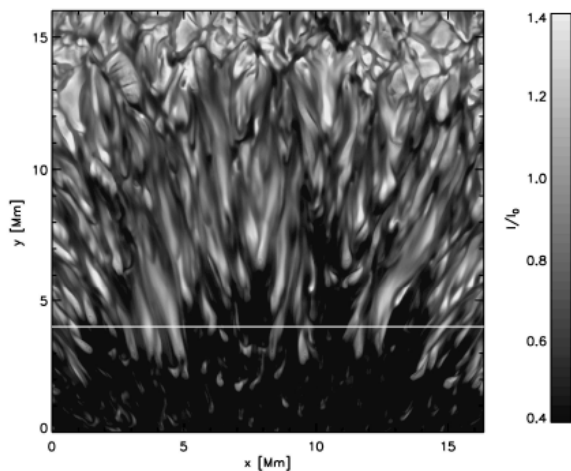


Fig. 8.— Bolometric intensity image of the penumbral section analyzed from the simulation of Rempel et al. (2009a); Rempel (2011). The white line indicates the slit position used for the time-slices shown in Fig. 9. An animation of this figure is available in the online journal.

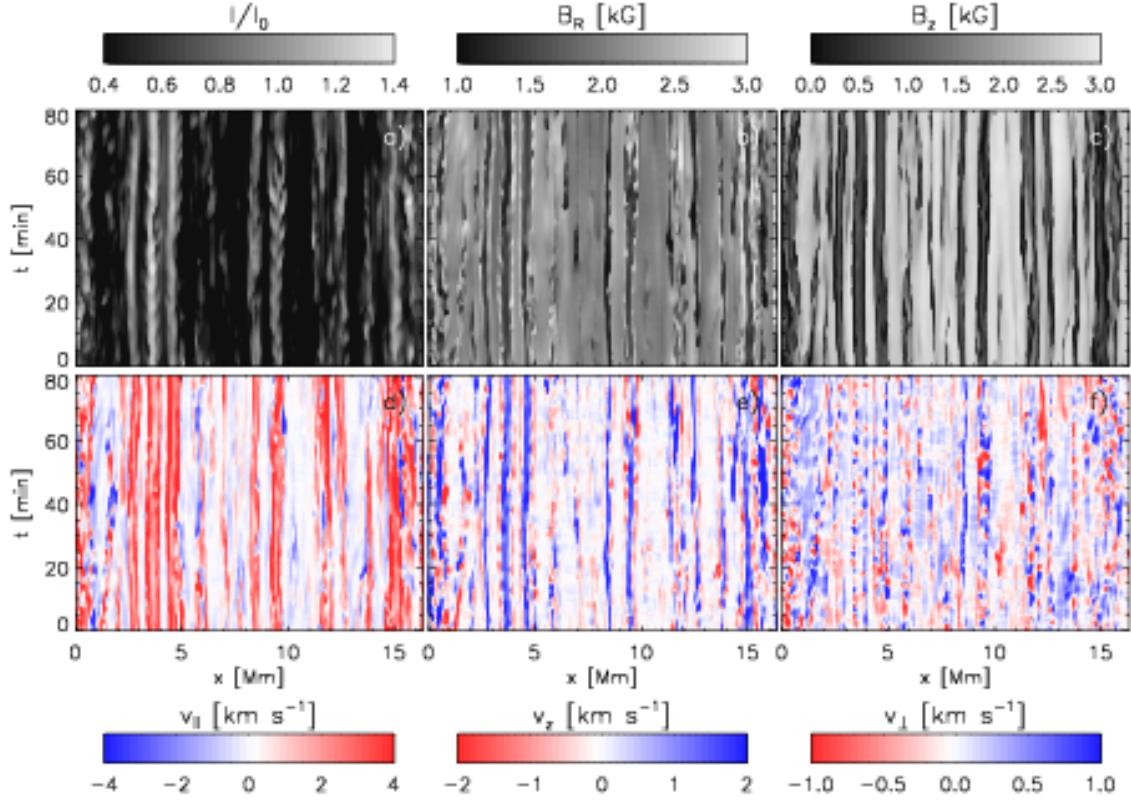


Fig. 9.— Space-time plots from the MHD simulation shown in Fig. 8. Shown are a) the bolometric intensity, b) strength of the magnetic field component in the radial direction (with respect to the approximate center of the spot), c) strength of the vertical magnetic field component, d) velocity component along the magnetic field’s direction (in the horizontal plane), e) vertical flow velocity, and f) velocity component perpendicular to magnetic field direction in the horizontal plane. Magnetic field and velocity data are for a constant geometric height $z = -300$ km below the average τ_{Ross} height of the quiet Sun.

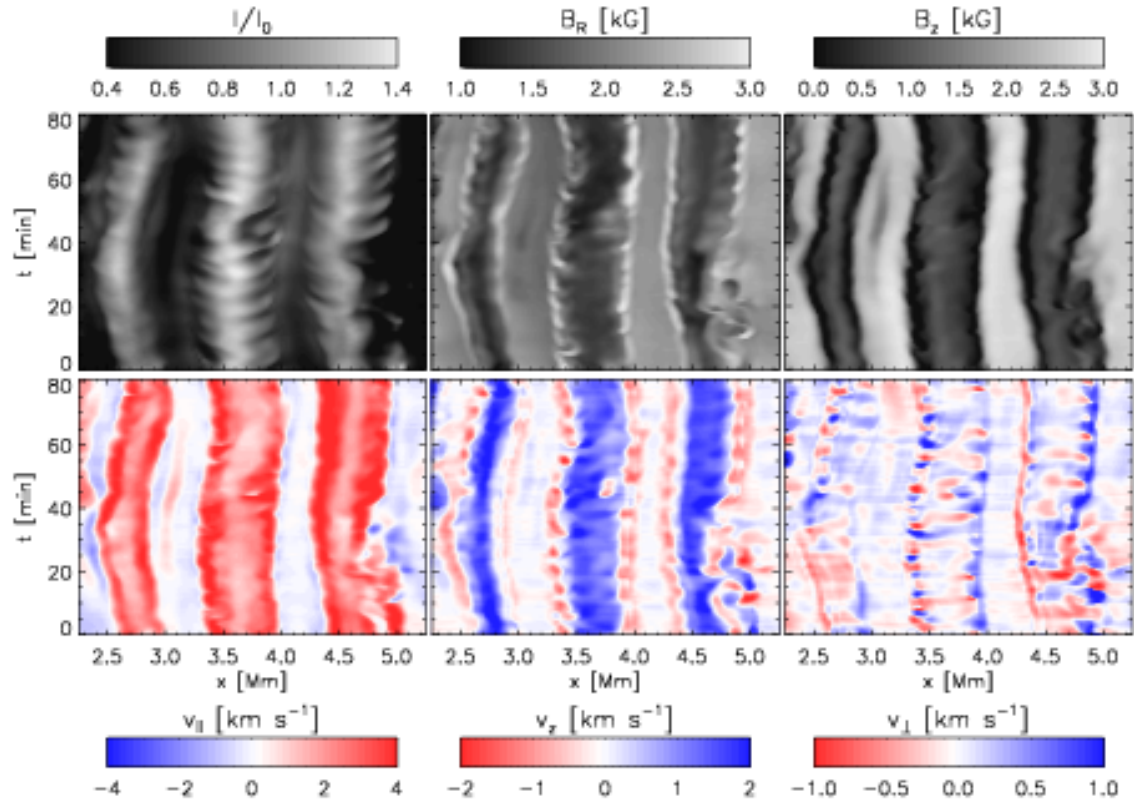


Fig. 10.— Same quantities as in Fig. 9 for the filaments located between $x = 2.25$ and $x = 5.25$ Mm.

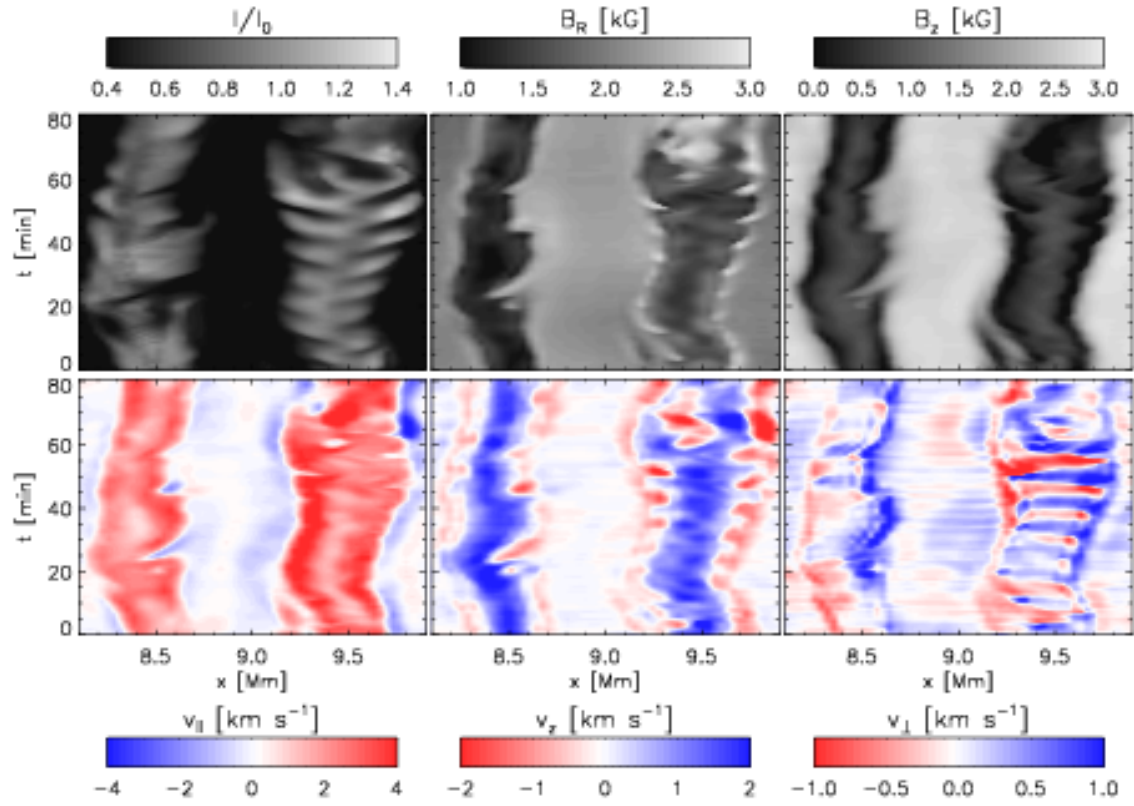


Fig. 11.— Same quantities as in Fig. 9 for the filaments located inbetween $x = 8.1$ and $x = 9.9$ Mm.

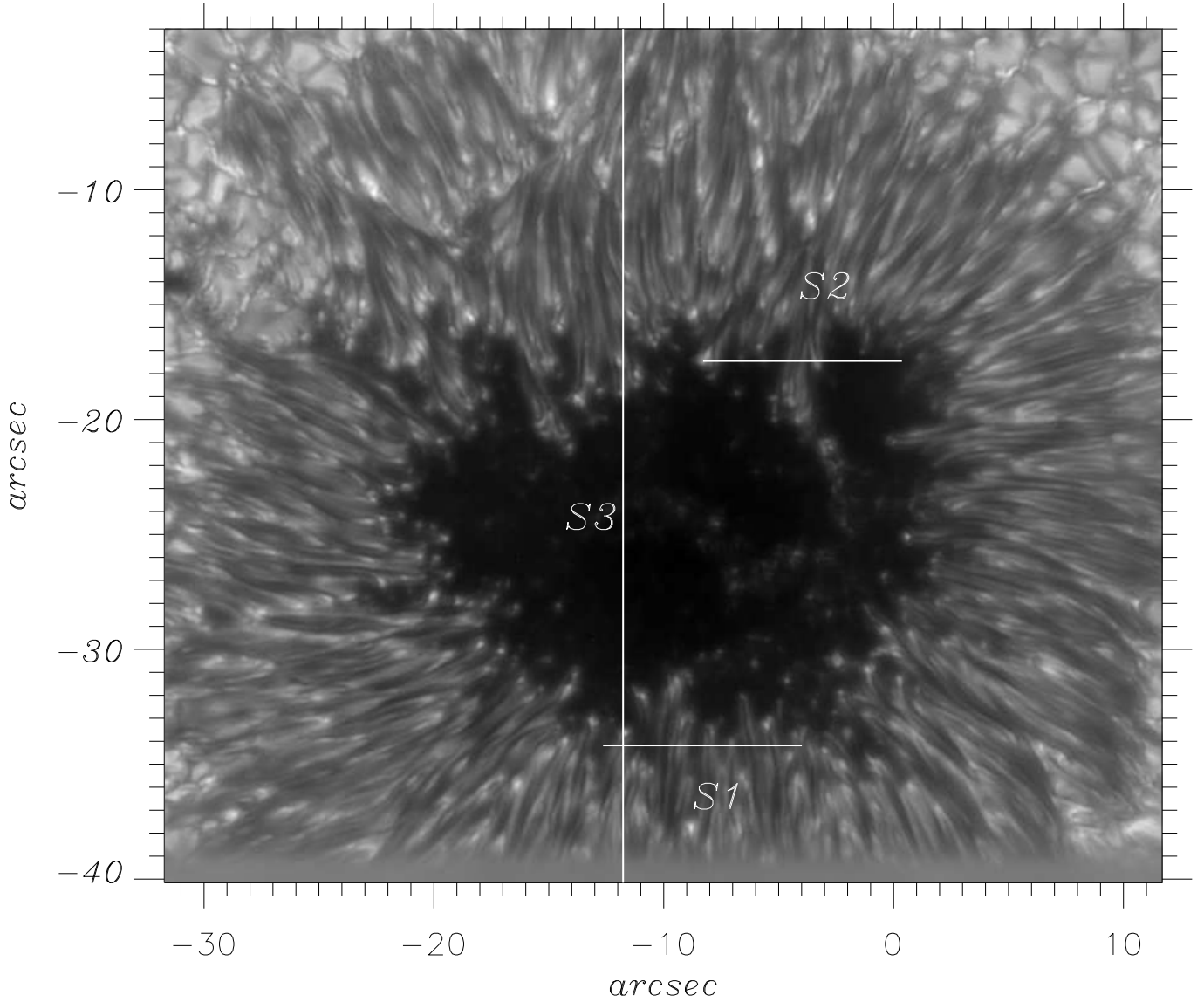


Fig. 12.— A sunspot image in the G-band taken on January 5, 2007 by the SOT/BFI aboard Hinode at disk center. 'S1' and 'S2' point to the locations of horizontal slits for which space-time diagrams have been made (see Figs. 13 and 15). Similarly 'S3' represents a vertical slit along which the space-time diagram displayed in Fig. 14 is constructed. Coordinate (0,0) corresponds to solar disc center.

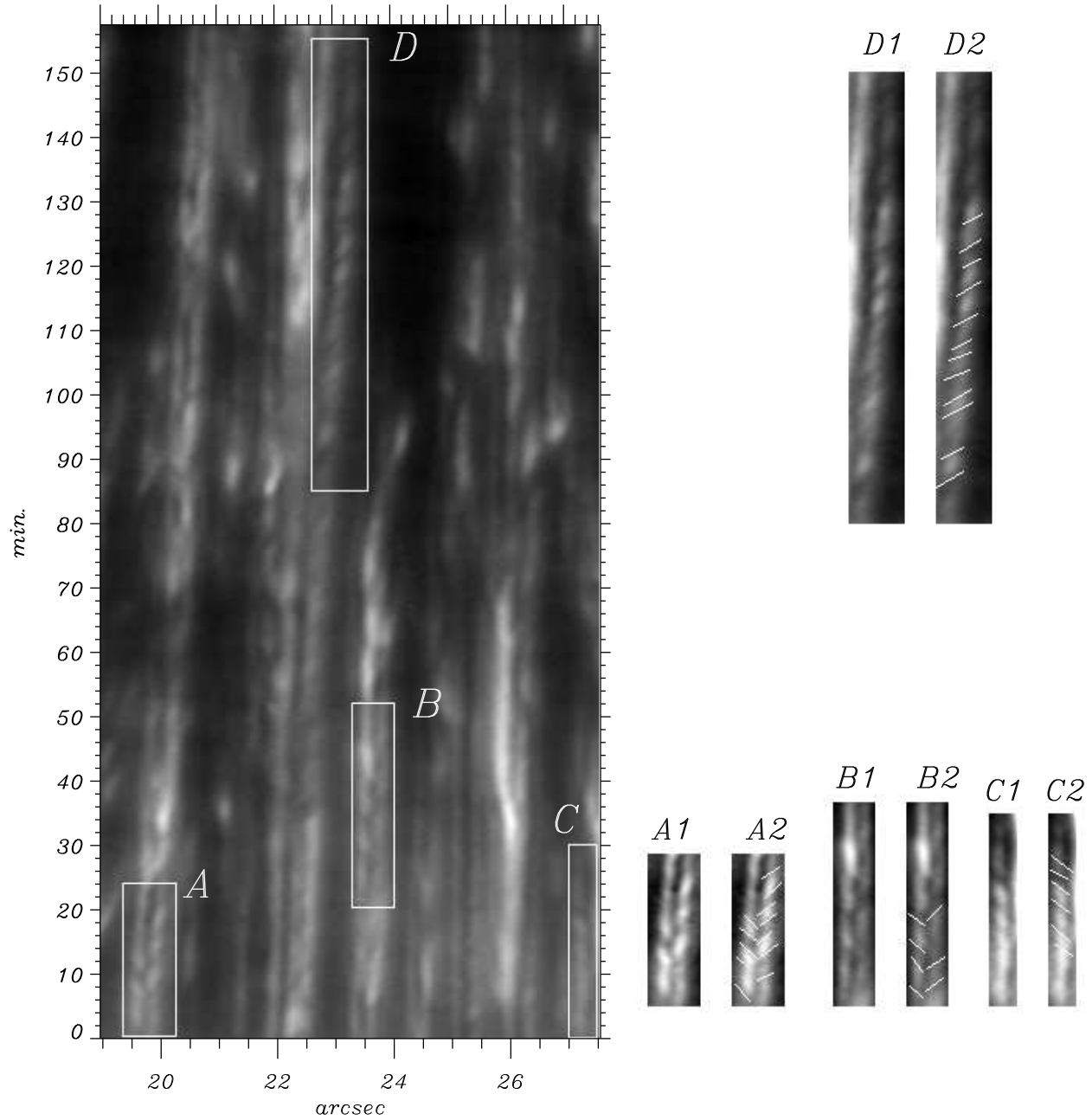


Fig. 13.— Large panel at left - Space-time slice along the line marked by 'S1' in Fig. 12. The highlighted boxes A, B, C and D are repeated in the small panels A1, B1, C1, D1. Panels A2, B2, C2, D2 repeat panels A1, B1, C1, D1, but with white lines overlying the dark stripes to better reveal their slopes, which are indicative of an apparent phase velocity.

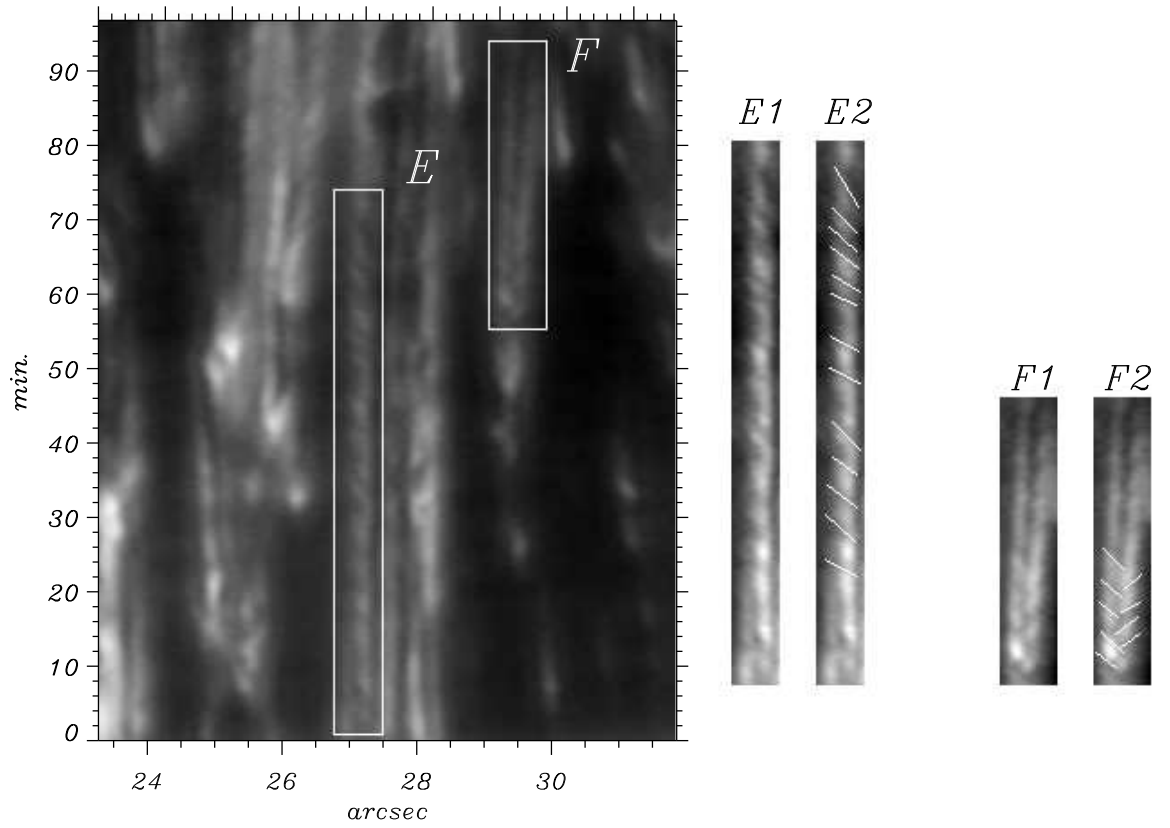


Fig. 14.— Same as Fig. 13, but along the line marked by 'S2' in Fig. 12.

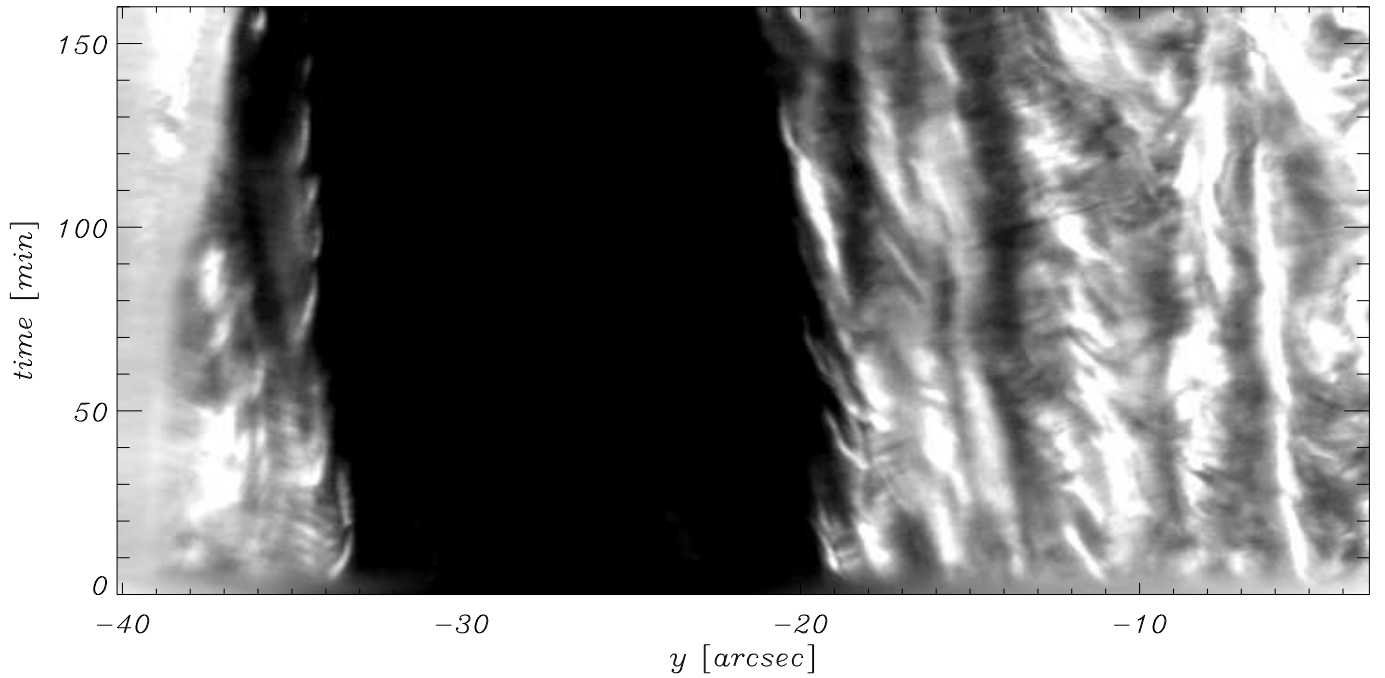


Fig. 15.— Space-time slice along the line marked by 'S3' in Fig. 12, almost along the filaments. The oscillations seen at $y = -35$ arcsec between $t = 0$ and $t = 30$ min are discussed in the main text.